ACS APPLIED ENERGY MATERIALS
Cite This: ACS Appl. Energy Mater. 2018, 1, 676−683
Article
www.acsaem.org

Preventing Hysteresis in Perovskite Solar Cells by Undoped Charge Blocking Layers

Nir Tessler*,† and Yana Vaynzof*,‡,§

†Sara and Moshe Zisapel Nano-Electronic Center, Department of Electrical Engineering, Technion-Israel Institute of Technology, Haifa 32000, Israel

‡Kirchhoff Institute for Physics, Heidelberg University, Im Neuenheimer Feld 227, 69120 Heidelberg, Germany

§Centre for Advanced Materials, Heidelberg University, Im Neuenheimer Feld 225, 69120 Heidelberg, Germany

Supporting Information

ABSTRACT: Preventing hysteresis in lead halide perovskite solar cells remains one of the key challenges hindering their integration into industrial applications. Herein, we numerically study a model solar cell system that is based on a mixed electron−ion conducting perovskite active layer and vary the configuration of undoped charge-blocking layers within the device. We find that the use of undoped blocking layers significantly reduces the potential drop across the perovskite active layer. This redistribution of voltage across the device suppresses the ion accumulation, or deficiency, which would otherwise develop at the two ends of the active layer. The fill factor is not compromised, provided that the blocking layers' mobility value is not lower than 0.01 $cm^2 V^{-1} s^{-1}$, which results in devices with power-conversion efficiencies surpassing 20% and minimal hysteresis. We believe that this method not only can suppress hysteresis effectively but could also contribute to the long-term stability of such cells that have been shown to be adversely affected by ion migration.

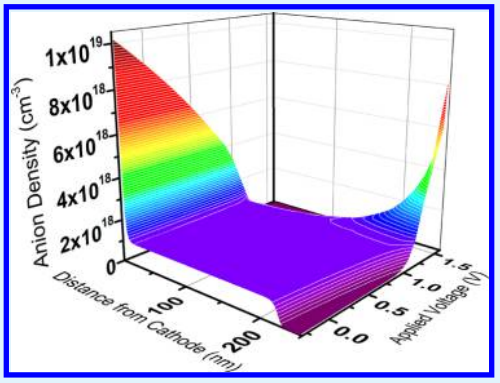

KEYWORDS: *perovskite solar cells, numerical simulations, ion migration, hysteresis, charge-blocking layers*

1. INTRODUCTION

The past years have witnessed rapid progress of metal halide perovskite solar cells,[1,2] with power-conversion efficiencies rising from below 10% to over 20%. Right from the start, different material combinations were studied[3] and some peculiarities of these cells were highlighted.[4] The progress has been so varied and so rapid that the reader is referred to several review articles recently published.[5−9] One of the remaining challenges is in understanding the role of the ions[10] on device operation, losses, and stability. This topic has been under investigation since the first reports of current−voltage hysteresis[11−13] and switchable photovoltaic effects in perovskite-based solar cells.[14,15] Among the various possible ions migrating throughout the perovskite layer (I^-, Pb^{2+}, and MA^+), it is generally accepted that I^- ions are the most mobile and dominate ion migration. Several theoretical works focused on the calculation of activation energy for each type of ion and concluded that I^- ions (anions) are more mobile than the cations.[16−18] The migration of I^- anions was confirmed experimentally by X-ray photoemission spectroscopy[10] and Kelvin probe force microscopy.[19,20]

In addition to being the most probable cause of device hysteresis, ion migration has also been linked to reduced device stability.[21,22] It is therefore of critical importance to elucidate the effect of ion migration on device performance and stability, as well as to develop mitigation strategies. Several approaches to suppress ion migration have been suggested, including passivation of grain boundary traps by fullerene diffusion,[23,24] improved crystallinity,[25] and the use of co-doping cations.[26]

Despite a wealth of experimental evidence for ion migration in perovskite solar cells, few reports on device modeling investigate the role of ions in device performance and stability.[27−31] In this contribution we expand our previous modeling of contacts[32,33] and blocking layers[34,35] to include ions and their electrostatic effects. We numerically study, using drift-diffusion and Poisson equations, a perovskite model system and focus on the role of charge-blocking layers (also called charge extraction layers) in such cells. We compare several device architectures and find that the use of undoped hole and electron-blocking layers allows one to engineer the field distribution across the device, significantly lowering the voltage drop across the ion conducting active layer. As a result, such a device architecture diminishes the hysteresis effect and results in high performance devices. Unlike the previously mentioned strategies for ion migration suppression, our method does not involve modifications to the perovskite active layer itself, which can be unfavorable due to its microstructure or optoelectronic properties.

Received: November 22, 2017
Accepted: February 6, 2018
Published: February 6, 2018

DOI: 10.1021/acsaem.7b00176
ACS Appl. Energy Mater. 2018, 1, 676−683

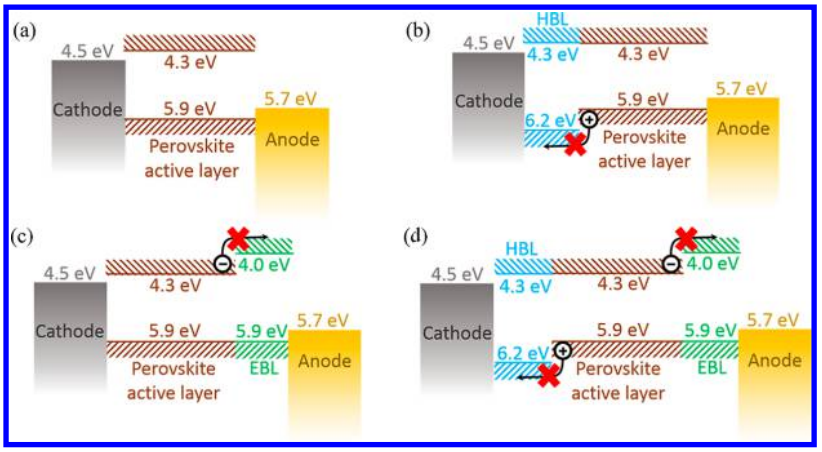

Figure 1. Schematic description of the structures used in the simulations. (a) Only the active (absorbing and ion conducting) layer with two metal contacts, (b) with added hole-blocking layer (HBL), (c) with added electron-blocking layer (EBL), and (d) with both HBL and EBL.

2. RESULTS AND DISCUSSION

2.1. Numerical Simulation Results. It is known that mixed conductor solar cells (e.g., lead halide perovskite cells) have the tendency to exhibit hysteresis in the current voltage response under light excitation.[4] To study this phenomena, we mimicked the experiments reported in ref 13 following the computational method reported in ref 27. The main difference with respect to ref 27 is that we focus on the role of the blocking layers (BLs), and we assume that the BLs are not doped. The details of the structures studied here are summarized in Figure 1. For simplicity, we assume that in all cases the contacts are 0.2 eV into the gap relative to the conducting level. We assume that the recombination losses are bimolecular[36] and low (10^{-5} relative to Langevin recombination),[27] as would be the case where the polycrystalline facets are efficiently passivated.[37,38] In agreement with both theoretical and experimental reports, we assume that ion migration is dominated by anions, whose mobility is considered to be significantly lower than that of charges. Other material parameters can be found in Table 1. We note that due to the numerical procedure and device structures used, one can swap roles between positive and negative charges and thus also observe the case where only cations, instead of anions, are mobile.

Table 1. Material Properties Used in the Simulations (Unless Stated Otherwise)

	active layer	blocking layer
electron/hole mobility ($cm^2v^{-1}s^{-1}$)	2	0.01
anion mobility	≪electron mobility	
cation mobility	0	
ion density (cm^{-3})	10^{18}	0
thickness (nm)	250	50

Figure 1a shows an active (absorbing and electron−ion conducting) layer sandwiched between two contacts. Panels b and c of Figure 1 show the structures where either a hole-blocking layer (HBL) or an electron-blocking layer (EBL) is introduced between the active layer and the respective contact. Figure 1d shows the structure of a balanced device with blocking layers on either side.

To obtain full steady state, or stabilized, $J-V$ curves, each bias point was solved until both the ions and the charges reached steady state. For the hysteresis calculations, the forward and backward scans in the [−0.4 V, 1.2 V] range were simulated separately (for schematic diagrams explaining the calculation procedure; see Supporting Information Figure S1). Specifically, the ions were first stabilized at −0.1 and 0.8 V for the forward and backward scans, respectively. During the scans, the ions were frozen to mimic a very fast scan and only charges were allowed to reach a new steady state.[13,27] The values for the stabilization points where chosen to be within the scanned range and were kept unchanged for all the device structures to allow for direct comparison. Since we decided not to use stabilized voltage that is well beyond the open circuit voltage (V_{OC}), we chose the upper value to match the lowest V_{OC} of all structures.

Figure 2a shows that devices structured without charge-blocking layers (orange line) result in pronounced hysteresis as well as a reduced V_{OC}. Panels b and c of Figure 2 show the results of the two asymmetric structures that include only a HBL (blue) or an EBL (green). It can be seen that having only one blocking layer is insufficient to diminish the hysteresis. Since only the anions are mobile, there is some difference depending on the type of blocking layer used. Additionally, we note that the fill factors of such asymmetric devices are reduced as a result of unbalanced charge extraction. Unlike the other structures, devices that incorporate both electron and hole-blocking layers (Figure 2d) show a ∼0.2 V increase in V_{OC} and nearly no hysteresis. The photovoltaic parameters of the reverse scans are summarized in Table 2.

The presence of hysteresis is also known to be associated with a reduction of the maximum power point. Figure 3 shows the stabilized $J-V$ curve with the maximum power points being marked with filled circles. The results presented in Figure 2 and Figure 3 have been previously reported in perovskite solar cell literature.[11−13] It is generally accepted that since the ions (anions here) remain mobile, regardless of the BLs, the effect of the BLs is to reduce recombination losses through the passivation of trap states at the surface and grain boundaries of perovskite polycrystalline films.[23,24] In the simulations reported here, however, the recombination constant is unchanged, with a low value (10^{-5} relative to Langevin's). Therefore, this suggests that the use of undoped BLs provides another mechanism to suppress hysteresis.

The differences in open circuit voltage of the four structures can be explained by changes in the dark current of the devices.

DOI: 10.1021/acsaem.7b00176
ACS Appl. Energy Mater. 2018, 1, 676−683

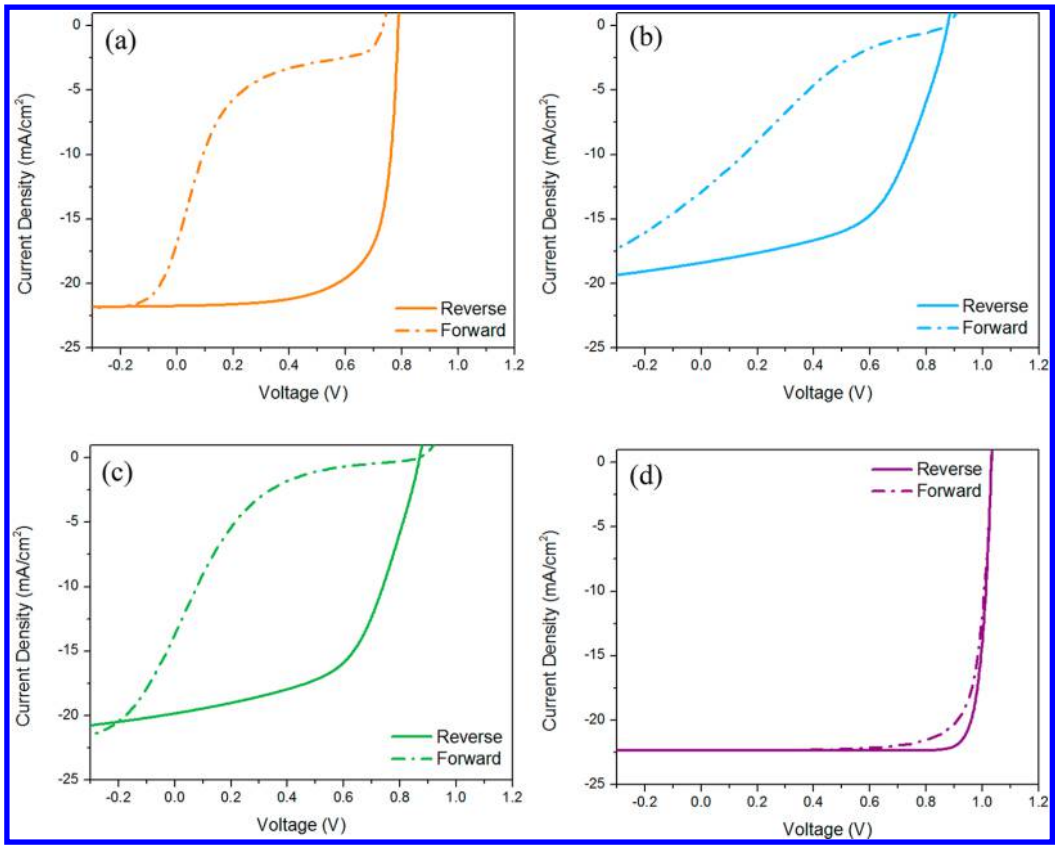

Figure 2. Current−voltage hysteresis calculated for devices with (a) no blocking layers, (b) devices with only HBL, (c) devices with only EBL, and (d) devices with both hole and electron-blocking layers. For all structures that include a blocking layer, the mobility in the BL was 10^{-2} cm^2 v^{-1} s^{-1}. For the forward (dashed line) and reverse (solid line) scans, the ions were first stabilized at −0.1 and 0.8 V, respectively. During the scans the ions were frozen to mimic a very fast scan.

Table 2. Photovoltaic Parameters of the Backwards Scans Presented in Figure 2

	J_{SC} (mA cm^{-2})	V_{OC} (V)	FF (%)	PCE (%)
no BL	21.8	0.8	70	12.2
EBL + HBL	22.4	1.05	86	20.2
HBL	19.85	0.88	55	9.6
EBL	18.4	0.88	55	8.9

This is because at V_{OC} the dark current and light generated current cancel each other. Figure 4 shows the stabilized dark current−voltage characteristics of the four structures. In general, a PN diode characteristic is described by

$$J = J_0\left[\exp\left(\frac{qV}{kT}\right) - 1\right]$$

with J_0 being the reverse saturation current and V the applied bias. The devices described here are not PN diodes but rather metal−insulator−metal (MIM) diodes. Such diodes when operated below the built-in potential also show a similar exponential rise.[39] However, in MIM diodes, the pre-exponent term J_0 is governed by the boundary conditions at the contacts and specifically the reverse injection barrier. To avoid confusion with the reverse saturation current of PN diodes, we will refer to J_0 as the reverse leakage current. If one extrapolates the exponential part (at $V > 0.2$ V) down to $V = 0$ V, the intercept with the y-axis ($V = 0$ V) is the reverse leakage current, J_0 (see inset of Figure 4). We note that adding one BL to the device structure only slightly reduces the leakage current, while the addition of both BLs significantly lowers it. This observation indicates that the leakage current J_0 is governed by the reverse injection at the contacts.[39] The incorporation of BLs enhances the reverse injection barrier and, as a result, reduces the reverse leakage current. As the reverse leakage current is directly associated with charge recombination at the contacts, under

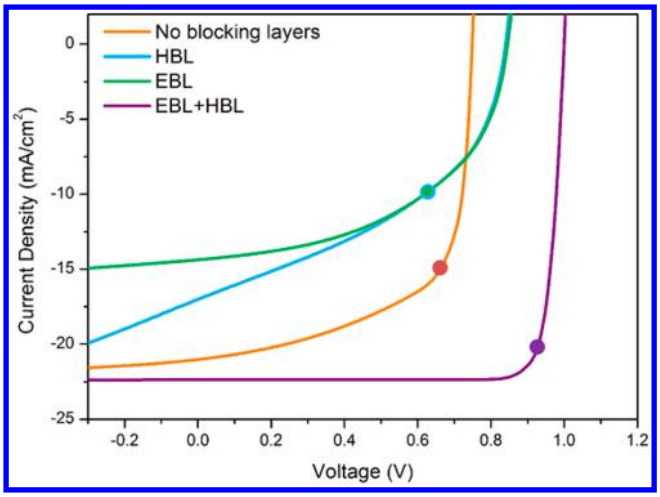

Figure 3. Stabilized current−voltage characteristics under one sun for the no BL (orange), HBL (blue), EBL (green), and HBL + EBL (purple) structures. The filled circles denote the maximum power point.

DOI: 10.1021/acsaem.7b00176
ACS Appl. Energy Mater. 2018, 1, 676−683

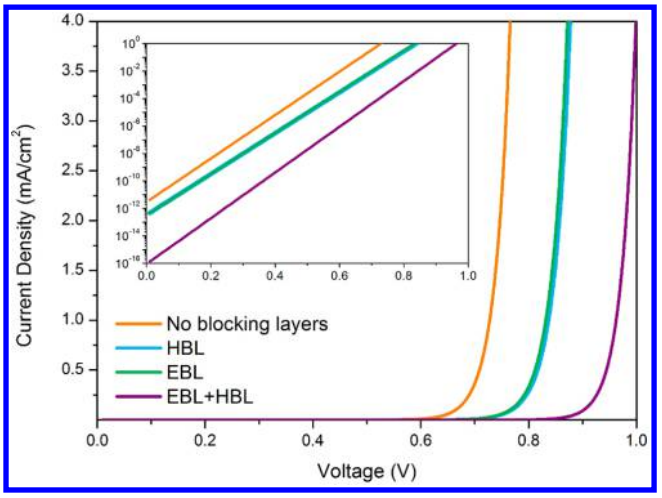

Figure 4. Dark current–voltage characteristics of the four structures: no blocking layers (orange), HBL or EBL only (blue, green), and both EBL and HBL (purple). The inset shows the extrapolation, toward V = 0 V, of the exponential part of the current. The intercept with the y-axis represents the reverse leakage current, J_0, which is significantly reduced for the EBL + HBL structure.

forward bias its reduction will lower this recombination rate and thus enhance V_{OC}.

To understand the differences in the shapes of the light J–V curves and the resulting hysteresis, it is useful to compare the potential and charge distribution across the device structure. Panels a–d of Figure 5 show the energy band diagrams of the four device structures as calculated for the stabilized maximum power point (full circles in Figure 3). We note that the voltage drops across the perovskite layer (0–250 nm) are 500, 160, 220, and 20 mV for the no BL (a), HBL (b), EBL (c), and HBL + EBL (d) structures, respectively. Namely, as we introduce undoped blocking layers, the voltage drop across the active layer is drastically decreased. It is also interesting to note that for the no BL device, the ion-induced band bending at the edges effectively creates carrier-blocking; however on the electron extracting side this is energetically far too low, at only 0.15 eV.

Panels d–f of Figure 5 show the electron and hole charge density distributions corresponding to Figure 5a–d. The device without any blocking layers is dominated by electrons, due to the ion migration-induced charge-blocking, which only efficiently blocks electrons at the anode (see Figure 5a). The very low hole density in the bulk of the active layer is a result of the high leakage of holes to the cathode. Introducing an undoped HBL (Figure 5b,f) turns the device into a hole dominated device, as the ion-induced blockage of electrons is removed. The low density of electrons now signifies the high electron leakage to the anode. Similarly, introducing an undoped EBL (Figure 5c,g) causes the device to be electron dominated, with the asymmetry between electrons and holes being more pronounced than previously (with respect to Figure 5f). Lastly, with the two BLs in place (Figure 5d,h), and since almost no voltage drops across the ion conducting layer, the device and charge distributions are symmetric and there is no evidence for significant leakage currents.

To complement the results presented in Figure 5, we show in Figure 6 the anion density distribution for the four structures at their maximum power point. The fact that adding undoped BLs shifts the voltage drop from the ion conducting layer to the BLs implies that fewer ions need to redistribute to compensate for the voltage drop across the ion conducting layer. The total excesses, or deficiencies, of anions close to the contacts are 1.5 $\times$ 10^{12}, 5.7 $\times$ 10^{11}, 7.5 $\times$ 10^{11}, and 6.5 $\times$ 10^{10} cm^{-2} for the no BL (purple), HBL (red), and HBL + EBL (green) structures, respectively. This reduction of almost 2 orders of magnitude is remarkable considering that no modifications were done to the active layer.

It is important to note that this effect does not occur in the case of doped blocking layers. To demonstrate this, we compared the potential distribution and ion density across a device with either two undoped or doped blocking layers (Supporting Information Figures S2 and S3). In the case of undoped BLs the total potential drop across the perovskite active layer is only 20 mV, while it is significantly larger in the

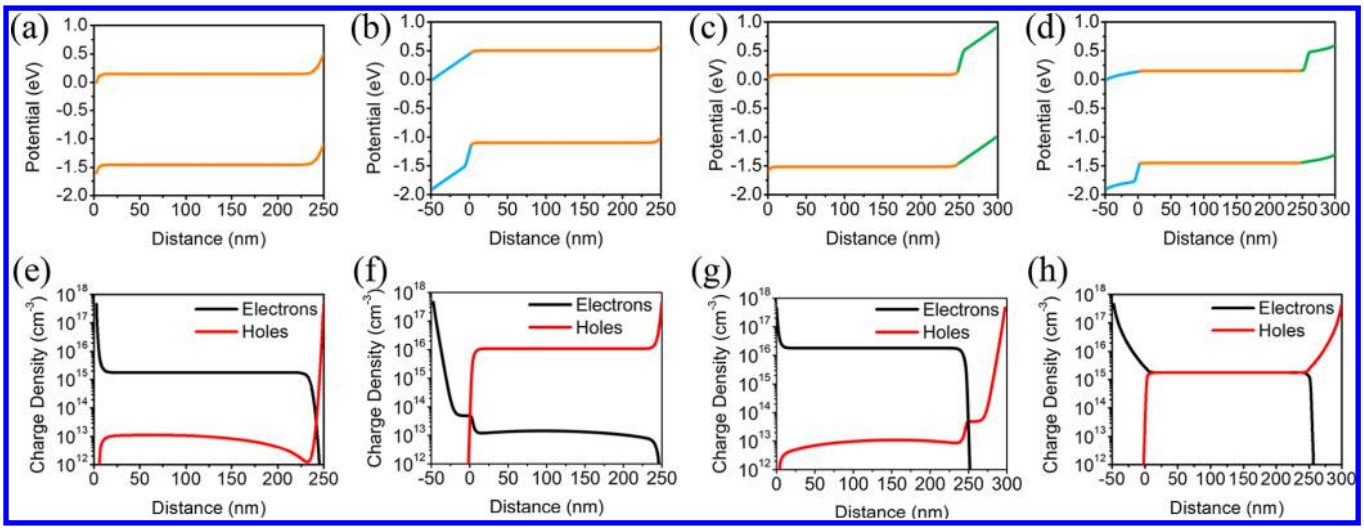

Figure 5. Energy band diagram at the stabilized maximum power point for the (a) no BL, (b) HBL only, (c) EBL only, and (d) HBL + EBL structures. (e–h) Corresponding electron and hole density distributions for the same structures as in panels a–d. The ion conducting layer is always plotted between 0 and 250 nm (orange), the potential across the HBL is shown between −50 and 0 nm (blue), and that across the EBL is between 250 and 300 nm (green). Note the very small voltage drop across the ion conducting layer of the EBL + HBL structure.

DOI: 10.1021/acsaem.7b00176
ACS Appl. Energy Mater. 2018, 1, 676–683

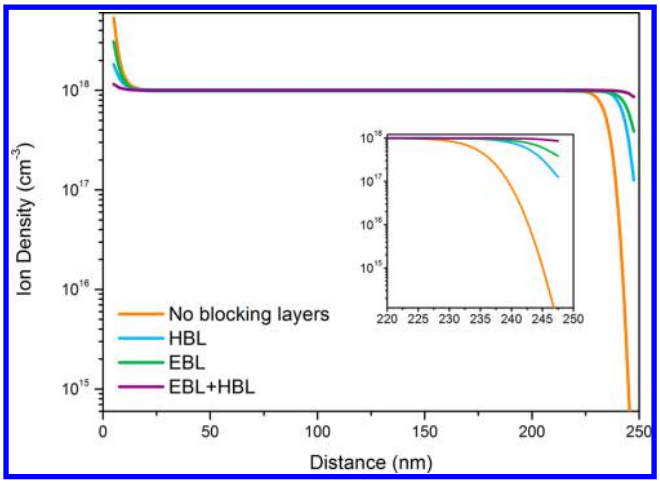

Figure 6. Anion distribution at the stabilized maximum power point for the no BL (orange), HBL (blue), EBL (green), and HBL + EBL (purple) structures. The inset is a zoom close to the anode side of the ion conducting layer. The respective ion accumulation densities are 1.5 × 10^{12}, 5.7 × 10^{11}, 7.5 × 10^{11}, and 6.5 × 10^{10} cm^{-2}.

case of doped BLs (180 mV). This increase in voltage drop across the active layer is a result of a decreased potential drop across the doped BLs. For example, the potential drop across an undoped HBL is 135 mV, far larger than for a doped HBL (30 mV). The total excess/deficiency of ions close to the contacts is therefore significantly increased in the case of doped BLs (Supporting Information Figure S3): as mentioned before, in the undoped case the total density is 6.5 × 10^{10} cm^{-2}, while doped blocking layers result in a total ion density of 5.5 × 10^{11} cm^{-2}. These results demonstrate that undoped blocking layers act as a mild serial resistance that reduces the voltage drop across the active layer, thus suppressing the ions' redistribution in the device.

2.2. Discussion. The applicability of our proposed method relies on the existence of materials that can, in their undoped form, serve as effective charge-blocking layers. Since the emergence of perovskite photovoltaics, a wide variety of charge-blocking layers have been investigated. In the standard architecture, most commonly the electron extracting layer consists of a solution processed metal oxide, such as TiO_2, ZnO, or SnO_2.[40−42] In their unmodified form, these layers are intrinsically n-doped and are highly understoichiometric.[43,44] Many studies exist that report on the intentional doping of metal oxide layers.[45−48] The hole extracting layer in these devices often consists of organic materials such as small molecules (most notably spiro-OMeTAD), or conjugated polymers (such as poly(3-hexylthiophene-2,5-diyl) (P3HT) or poly[*N*-9-heptadecanyl-2,7-carbazole-*alt*-3,6-bis(thiophen-5-yl)-2,5-dioctyl-2,5-dihydropyrrolo[3,4-]pyrrole-1,4-dione] (PCBTDPP)[49]). Spiro-OMeTAD remains the most ubiquitously used hole transporting material; however, it requires doping by lithium bis(trifluoromethanesulfonyl)imide (Li-TFSI)[50] and subsequent doping with oxygen and water.[51] Although polymers such as P3HT can be also used in their undoped form,[52] their performance is inferior to other hole transporting materials and can only be improved by doping.[53]

In inverted architecture devices, hole extraction is commonly obtained by using doped poly(3,4-ethylenedioxythiophene) polystyrenesulfonate (PEDOT:PSS).[54,55] Other examples include undoped polymeric hole transporters such as poly[*N*,*N*-bis(4-butylphenyl)-*N*,*N*-bis(phenyl)benzidine] (poly-TPD) and poly(triarylamine) (PTAA)[56] or inorganic hole transporters such as CuSCN[57] and NiO.[58] Efficient electron extraction is achieved by using fullerenes such as C60 or PCBM.[59]

Although the vast majority of reported extraction layers are doped in some way, some reports have focused on the development of undoped charge transport layers. For example, Kazim et al. demonstrated the use of TIPS−pentacene as an efficient undoped hole extraction layer.[60] Qin and co-workers reported on the synthesis and application of quinolizino acridine-based hole transporting materials, or alternatively that of *S*,*N*-heteroacene-based oligothiophenes.[61,62] These examples, or the previously mentioned poly-TPD or PTAA, can all serve as undoped hole extraction layers.

In the case of dopant-free small molecule electron extracting layers, in addition to the commonly used fullerenes, planar coronenes have also been utilized in perovskite photovoltaic devices with negligible hysteresis.[63] A variety of hexaazatrinaphthylene derivatives were investigated by Zhao and co-workers, resulting in comparable performance to that of PCBM.[64] Recently, Gu et al. demonstrated that the use of sulfur-containing azaacene can result in devices surpassing the efficiency of those with fullerene electron extraction layers.[65] Significantly fewer examples of the use of conjugated polymers as electron extraction layers exist; however, two amino-functionalized conjugated polymers have also been reported.[66]

One concern that may arise from the use of undoped extraction layers is the limitation on charge transport in the absence of dopants. Indeed, the key reason why commonly used materials such as spiro-OMeTAD are doped is to increase their conductivity.[51] We have investigated the importance of mobility in our model and varied the charge carrier mobility of the undoped extraction layers from 10^{-4} to 10^{-2} cm^2 V^{-1} s^{-1}. We find that low mobility results in inefficient charge extraction, such that noticeable hysteresis is present (Supporting Information Figure S4). However, at higher mobility values of 10^{-2} cm^2 V^{-1} s^{-1}, high performance is obtained and nearly no hysteresis can be observed. This mobility value is reasonable for the various undoped extraction layers discussed above. As a result, charge transport should not be a limiting factor in the application of our results.

The use of thin charge extraction layers might prove detrimental to large area solar cell fabrication techniques, such as printing. To explore this, we investigated the role of blocking layer thickness on the performance and hysteresis of perovskite solar cells and found that, in the case of undoped layers, thicker layers result in equally good performance (Supporting Information Figure S5) and minimal ion distribution (Supporting Information Figure S6). These results further demonstrate the potential of our approach to be used in a range of device architectures deposited by various methods.

The suppression of ion migration not only should result in hysteresis-free photovoltaic performance but is also expected to have a positive influence on device stability. For example, several reports show that device degradation occurs due to the Ag electrode reacting with I^- to form AgI.[22,67] Other reports show that the presence of iodine within the charge transport layers can also serve as a device degradation mechanism.[68] Iodine migration within the perovskite active layer itself has also been linked to reduced stability.[16] To improve device stability, it has been proposed that suppressing ion migration through charge extraction layers can be achieved by incorporating N-doped graphene,[69] or bilayered Al-doped

DOI: 10.1021/acsaem.7b00176
ACS Appl. Energy Mater. 2018, 1, 676−683

ZnO/SnOx, into the device architecture.[70] Suppressing ion migration through the use of undoped extraction layers, as proposed here, would serve as an alternative strategy, potentially eliminating the need to introduce additional impermeable layers that complicate device fabrication.

3. CONCLUSION

To summarize, we have investigated the effect of introducing undoped charge-blocking layers on ion migration in perovskite photovoltaic devices. To accomplish this, several device configurations that include or exclude charge-blocking layers were used as a model system to numerically solve the ion and potential distribution throughout the device. We find that a symmetric architecture that incorporates undoped hole and electron extraction layers results in an advantageous potential redistribution across the device, such that nearly no field is present within the perovskite layer or at its edges. This suppresses the field-induced ion migration within the perovskite layer, and lowers the density of accumulated ions by 2 orders of magnitude, without any modifications to the perovskite layer. Due to the large variety of materials that can be used as undoped layers, we believe our method can be applied to functional photovoltaic devices and should result in improved performance, elimination of hysteresis, and enhanced long-term stability.

■ ASSOCIATED CONTENT

Supporting Information

The Supporting Information is available free of charge on the ACS Publications website at DOI: 10.1021/acsaem.7b00176.

Device model description, procedure for hysteresis calculations, comparing doped and undoped BLs, effect of electron/hole mobility of the blocking layers and effect of blocking layer thickness, effect of scan rate, and simulations that do not include ions (PDF)

■ AUTHOR INFORMATION

Corresponding Authors

*E-mail: nir@ef.technion.ac.il (N.T.).
*E-mail: vaynzof@uni-heidelberg.de (Y.V.).

ORCID

Yana Vaynzof: 0000-0002-0783-0707

Notes

The authors declare no competing financial interest.

■ ACKNOWLEDGMENTS

We acknowledge fruitful discussion with David Cahen. N.T. acknowledges support by the Israel Science Foundation (Grant No. 488/16) and the Adelis Foundation for renewable energy research within the framework of the Grand Technion Energy Program (GTEP).

■ REFERENCES

(1) Lee, M. M.; Teuscher, J.; Miyasaka, T.; Murakami, T. N.; Snaith, H. J. Efficient Hybrid Solar Cells Based on Meso-Superstructured Organometal Halide Perovskites. *Science* **2012**, *338*, 643−647.

(2) Burschka, J.; Pellet, N.; Moon, S.-J.; Humphry-Baker, R.; Gao, P.; Nazeeruddin, M. K.; Gratzel, M. Sequential Deposition as a Route to High-Performance Perovskite-Sensitized Solar Cells. *Nature* **2013**, *499*, 316−319.

(3) Edri, E.; Kirmayer, S.; Cahen, D.; Hodes, G. High Open-Circuit Voltage Solar Cells Based on Organic−Inorganic Lead Bromide Perovskite. *J. Phys. Chem. Lett.* **2013**, *4*, 897−902.

(4) Unger, E. L.; Hoke, E. T.; Bailie, C. D.; Nguyen, W. H.; Bowring, A. R.; Heumuller, T.; Christoforo, M. G.; McGehee, M. D. Hysteresis and Transient Behavior in Current−Voltage Measurements of Hybrid-Perovskite Absorber Solar Cells. *Energy Environ. Sci.* **2014**, *7*, 3690−3698.

(5) Brenner, T. M.; Egger, D. A.; Kronik, L.; Hodes, G.; Cahen, D. Hybrid Organic-Inorganic Perovskites: Low-Cost Semiconductors with Intriguing Charge-Transport Properties. *Nat. Rev. Mater.* **2016**, *1*, 15007.

(6) Yang, S.; Fu, W.; Zhang, Z.; Chen, H.; Li, C.-Z. Recent Advances in Perovskite Solar Cells: Efficiency, Stability and Lead-Free Perovskite. *J. Mater. Chem. A* **2017**, *5*, 11462−11482.

(7) Manser, J. S.; Christians, J. A.; Kamat, P. V. Intriguing Optoelectronic Properties of Metal Halide Perovskites. *Chem. Rev.* **2016**, *116*, 12956−13008.

(8) Gottesman, R.; Zaban, A. Perovskites for Photovoltaics in the Spotlight: Photoinduced Physical Changes and Their Implications. *Acc. Chem. Res.* **2016**, *49*, 320−329.

(9) Amgar, D.; Aharon, S.; Etgar, L. Inorganic and Hybrid Organo-Metal Perovskite Nanostructures: Synthesis, Properties, and Applications. *Adv. Funct. Mater.* **2016**, *26*, 8576−8593.

(10) Li, C.; Tscheuschner, S.; Paulus, F.; Hopkinson, P. E.; Kießling, J.; Köhler, A.; Vaynzof, Y.; Huettner, S. Iodine Migration and its Effect on Hysteresis in Perovskite Solar Cells. *Adv. Mater.* **2016**, *28*, 2446−2454.

(11) Snaith, H. J.; Abate, A.; Ball, J. M.; Eperon, G. E.; Leijtens, T.; Noel, N. K.; Stranks, S. D.; Wang, J. T.-W.; Wojciechowski, K.; Zhang, W. Anomalous Hysteresis in Perovskite Solar Cells. *J. Phys. Chem. Lett.* **2014**, *5*, 1511−1515.

(12) Jeon, N. J.; Noh, J. H.; Kim, Y. C.; Yang, W. S.; Ryu, S.; Seok, S. I. Solvent Engineering for High-Performance Inorganic−Organic Hybrid Perovskite Solar Cells. *Nat. Mater.* **2014**, *13*, 897−903.

(13) Tress, W.; Marinova, N.; Moehl, T.; Zakeeruddin, S. M.; Nazeeruddin, M. K.; Gratzel, M. Understanding the Rate-Dependent J−V Hysteresis, Slow Time Component, and Aging in $CH_3NH_3PbI_3$ Perovskite Solar Cells: the Role of a Compensated Electric Field. *Energy Environ. Sci.* **2015**, *8*, 995−1004.

(14) Xiao, Z.; Yuan, Y.; Shao, Y.; Wang, Q.; Dong, Q.; Bi, C.; Sharma, P.; Gruverman, A.; Huang, J. Giant Switchable Photovoltaic Effect in Organometal Trihalide Perovskite Devices. *Nat. Mater.* **2015**, *14*, 193−198.

(15) Gottesman, R.; Haltzi, E.; Gouda, L.; Tirosh, S.; Bouhadana, Y.; Zaban, A.; Mosconi, E.; De Angelis, F. Extremely Slow Photoconductivity Response of CH3NH3PbI3 Perovskites Suggesting Structural Changes under Working Conditions. *J. Phys. Chem. Lett.* **2014**, *5*, 2662−2669.

(16) Eames, C.; Frost, J. M.; Barnes, P. R. F.; O'Regan, B. C.; Walsh, A.; Islam, M. S. Ionic Transport in Hybrid Lead Iodide Perovskite Solar Cells. *Nat. Commun.* **2015**, *6*, 7497.

(17) Azpiroz, J. M.; Mosconi, E.; Bisquert, J.; De Angelis, F. Defect Migration in Methylammonium Lead Iodide and its Role in Perovskite Solar Cell Operation. *Energy Environ. Sci.* **2015**, *8*, 2118−2127.

(18) Haruyama, J.; Sodeyama, K.; Han, L.; Tateyama, Y. First-Principles Study of Ion Diffusion in Perovskite Solar Cell Sensitizers. *J. Am. Chem. Soc.* **2015**, *137*, 10048−10051.

(19) Yuan, Y.; Wang, Q.; Shao, Y.; Lu, H.; Li, T.; Gruverman, A.; Huang, J. Electric-Field-Driven Reversible Conversion Between Methylammonium Lead Triiodide Perovskites and Lead Iodide at Elevated Temperatures. *Adv. Energy Mater.* **2016**, *6*, 1501803.

(20) Yang, B.; Brown, C. C.; Huang, J.; Collins, L.; Sang, X.; Unocic, R. R.; Jesse, S.; Kalinin, S. V.; Belianinov, A.; Jakowski, J.; Geohegan, D. B.; Sumpter, B. G.; Xiao, K.; Ovchinnikova, O. S. Enhancing Ion Migration in Grain Boundaries of Hybrid Organic−Inorganic Perovskites by Chlorine. *Adv. Funct. Mater.* **2017**, *27*, 1700749.

(21) Hoke, E. T.; Slotcavage, D. J.; Dohner, E. R.; Bowring, A. R.; Karunadasa, H. I.; McGehee, M. D. Reversible Photo-Induced Trap

DOI: 10.1021/acsaem.7b00176
ACS Appl. Energy Mater. 2018, 1, 676−683

Formation in Mixed-Halide Hybrid Perovskites for Photovoltaics. *Chem. Sci.* **2015**, *6*, 613−617.
(22) Besleaga, C.; Abramiuc, L. E.; Stancu, V.; Tomulescu, A. G.; Sima, M.; Trinca, L.; Plugaru, N.; Pintilie, L.; Nemnes, G. A.; Iliescu, M.; Svavarsson, H. G.; Manolescu, A.; Pintilie, I. Iodine Migration and Degradation of Perovskite Solar Cells Enhanced by Metallic Electrodes. *J. Phys. Chem. Lett.* **2016**, *7*, 5168−5175.
(23) Shao, Y.; Xiao, Z.; Bi, C.; Yuan, Y.; Huang, J. Origin and Elimination of Photocurrent Hysteresis by Fullerene Passivation in $CH_3NH_3PbI_3$ Planar Heterojunction Solar Cells. *Nat. Commun.* **2014**, *5*, 5784.
(24) Xu, J.; Buin, A.; Ip, A. H.; Li, W.; Voznyy, O.; Comin, R.; Yuan, M.; Jeon, S.; Ning, Z.; McDowell, J. J.; Kanjanaboos, P.; Sun, J.-P.; Lan, X.; Quan, L. N.; Kim, D. H.; Hill, I. G.; Maksymovych, P.; Sargent, E. H. Perovskite−Fullerene Hybrid Materials Suppress Hysteresis in Planar Diodes. *Nat. Commun.* **2015**, *6*, 7081.
(25) Hu, M.; Bi, C.; Yuan, Y.; Bai, Y.; Huang, J. Stabilized Wide Bandgap $MAPbBr_xI_{3-x}$ Perovskite by Enhanced Grain Size and Improved Crystallinity. *Adv. Sci.* **2016**, *3*, 1500301.
(26) Kharton, V. V.; Viskup, A. P.; Yaremchenko, A. A.; Baker, R. T.; Gharbage, B.; Mather, G. C.; Figueiredo, F. M.; Naumovich, E. N.; Marques, F. M. B. Ionic Conductivity of $La(Sr)Ga(Mg,M)O_{3-\delta}$ (M = Ti, Cr, Fe, Co, Ni): Effects of Transition Metal Dopants. *Solid State Ionics* **2000**, *132*, 119−130.
(27) van Reenen, S.; Kemerink, M.; Snaith, H. J. Modeling Anomalous Hysteresis in Perovskite Solar Cells. *J. Phys. Chem. Lett.* **2015**, *6*, 3808−3814.
(28) O'Kane, S. E. J.; Richardson, G.; Pockett, A.; Niemann, R. G.; Cave, J. M.; Sakai, N.; Eperon, G. E.; Snaith, H. J.; Foster, J. M.; Cameron, P. J.; Walker, A. B. Measurement and Modelling of Dark Current Decay Transients in Perovskite Solar Cells. *J. Mater. Chem. C* **2017**, *5*, 452−462.
(29) Richardson, G.; O'Kane, S. E. J.; Niemann, R. G.; Peltola, T. A.; Foster, J. M.; Cameron, P. J.; Walker, A. B. Can Slow-Moving Ions Explain Hysteresis in the Current−Voltage Curves of Perovskite Solar Cells? *Energy Environ. Sci.* **2016**, *9*, 1476−1485.
(30) Sherkar, T. S.; Momblona, C.; Gil-Escrig, L.; Bolink, H. J.; Koster, L. J. A. Improving Perovskite Solar Cells: Insights From a Validated Device Model. *Adv. Energy Mater.* **2017**, *7*, 1602432.
(31) Huang, Y.; Aharon, S.; Rolland, A.; Pedesseau, L.; Durand, O.; Etgar, L.; Even, J. Influence of Schottky Contact on the C-V and J-V Characteristics of HTM-Free Perovskite Solar Cells. *EPJ Photovoltaics* **2017**, *8*, 85501.
(32) Tessler, N. The Band-Gap Enhanced Photovoltaic Structure. *Appl. Phys. Lett.* **2016**, *108*, 183503.
(33) Tessler, N. Adding 0.2V to the Open Circuit Voltage of Organic Solar Cells by Enhancing the Built-in Potential. *J. Appl. Phys.* **2015**, *118*, 215501.
(34) Magen, O.; Tessler, N. On Electrode Pinning and Charge Blocking Layers in Organic Solar Cells. *J. Appl. Phys.* **2017**, *121*, 195502.
(35) Hinzmann, C.; Magen, O.; Hofstetter, Y. J.; Hopkinson, P. E.; Tessler, N.; Vaynzof, Y. Effect of Injection Layer Sub-Bandgap States on Electron Injection in Organic Light-Emitting Diodes. *ACS Appl. Mater. Interfaces* **2017**, *9*, 6220−6227.
(36) Deschler, F.; Price, M.; Pathak, S.; Klintberg, L. E.; Jarausch, D.-D.; Higler, R.; Hüttner, S.; Leijtens, T.; Stranks, S. D.; Snaith, H. J.; Atatüre, M.; Phillips, R. T.; Friend, R. H. High Photoluminescence Efficiency and Optically Pumped Lasing in Solution-Processed Mixed Halide Perovskite Semiconductors. *J. Phys. Chem. Lett.* **2014**, *5*, 1421−1426.
(37) deQuilettes, D. W.; Koch, S.; Burke, S.; Paranji, R. K.; Shropshire, A. J.; Ziffer, M. E.; Ginger, D. S. Photoluminescence Lifetimes Exceeding 8 μs and Quantum Yields Exceeding 30% in Hybrid Perovskite Thin Films by Ligand Passivation. *ACS Energy Lett.* **2016**, *1*, 438−444.
(38) De Marco, N.; Zhou, H.; Chen, Q.; Sun, P.; Liu, Z.; Meng, L.; Yao, E.-P.; Liu, Y.; Schiffer, A.; Yang, Y. Guanidinium: A Route to Enhanced Carrier Lifetime and Open-Circuit Voltage in Hybrid Perovskite Solar Cells. *Nano Lett.* **2016**, *16* (2), 1009−1016.
(39) Nguyen, P. H.; Scheinert, S.; Berleb, S.; Brütting, W.; Paasch, G. The influence of deep traps on transient current−voltage characteristics of organic light-emitting diodes. *Org. Electron.* **2001**, *2*, 105−120.
(40) Liu, D.; Kelly, T. L. Perovskite Solar Cells with a Planar Heterojunction Structure Prepared using Room-Temperature Solution Processing Techniques. *Nat. Photonics* **2014**, *8*, 133−138.
(41) McMeekin, D. P.; Sadoughi, G.; Rehman, W.; Eperon, G. E.; Saliba, M.; Hörantner, M. T.; Haghighirad, A.; Sakai, N.; Korte, L.; Rech, B.; Johnston, M. B.; Herz, L. M.; Snaith, H. J. A Mixed-Cation Lead Mixed-Halide Perovskite Absorber for Tandem Solar Cells. *Science* **2016**, *351*, 151−155.
(42) Anaraki, E. H.; Kermanpur, A.; Steier, L.; Domanski, K.; Matsui, T.; Tress, W.; Saliba, M.; Abate, A.; Gratzel, M.; Hagfeldt, A.; Correa-Baena, J.-P. Highly Efficient and Stable Planar Perovskite Solar Cells by Solution-Processed Tin Oxide. *Energy Environ. Sci.* **2016**, *9*, 3128−3134.
(43) Janotti, A.; Van de Walle, C. G. Fundamentals of Zinc Oxide as a Semiconductor. *Rep. Prog. Phys.* **2009**, *72*, 126501.
(44) Morgan, B. J.; Watson, G. W. Intrinsic n-type Defect Formation in TiO_2: A Comparison of Rutile and Anatase from GGA+U Calculations. *J. Phys. Chem. C* **2010**, *114*, 2321−2328.
(45) Zhou, H.; Chen, Q.; Li, G.; Luo, S.; Song, T.-b.; Duan, H.-S.; Hong, Z.; You, J.; Liu, Y.; Yang, Y. Interface Engineering of Highly Efficient Perovskite Solar Cells. *Science* **2014**, *345*, 542−546.
(46) Kim, D. H.; Han, G. S.; Seong, W. M.; Lee, J.-W.; Kim, B. J.; Park, N.-G.; Hong, K. S.; Lee, S.; Jung, H. S. Niobium Doping Effects on TiO_2 Mesoscopic Electron Transport Layer-Based Perovskite Solar Cells. *ChemSusChem* **2015**, *8*, 2392−2398.
(47) An, Q.; Fassl, P.; Hofstetter, Y. J.; Becker-Koch, D.; Bausch, A.; Hopkinson, P. E.; Vaynzof, Y. High Performance Planar Perovskite Solar Cells by ZnO Electron Transport Layer Engineering. *Nano Energy* **2017**, *39*, 400−408.
(48) Pathak, S. K.; Abate, A.; Ruckdeschel, P.; Roose, B.; Gödel, K. C.; Vaynzof, Y.; Santhala, A.; Watanabe, S.-I.; Hollman, D. J.; Noel, N.; Sepe, A.; Wiesner, U.; Friend, R. H.; Snaith, H. J.; Steiner, U. Performance and Stability Enhancement of Dye-Sensitized and Perovskite Solar Cells by Al Doping of TiO_2. *Adv. Funct. Mater.* **2014**, *24*, 6046−6055.
(49) Cai, B.; Xing, Y.; Yang, Z.; Zhang, W.-H.; Qiu, J. High Performance Hybrid Solar Cells Sensitized by Organolead Halide Perovskites. *Energy Environ. Sci.* **2013**, *6*, 1480−1485.
(50) Zhang, H.; Shi, Y.; Yan, F.; Wang, L.; Wang, K.; Xing, Y.; Dong, Q.; Ma, T. A Dual Functional Additive for the HTM Layer in Perovskite Solar Cells. *Chem. Commun.* **2014**, *50*, 5020−5022.
(51) Hawash, Z.; Ono, L. K.; Qi, Y. Moisture and Oxygen Enhance Conductivity of LiTFSI-Doped Spiro-MeOTAD Hole Transport Layer in Perovskite Solar Cells. *Adv. Mater. Interfaces* **2016**, *3*, 1600117.
(52) Nia, N. Y.; Matteocci, F.; Cina, L.; Di Carlo, A. High-Efficiency Perovskite Solar Cell Based on Poly(3-Hexylthiophene): Influence of Molecular Weight and Mesoscopic Scaffold Layer. *ChemSusChem* **2017**, *10*, 3854−3860.
(53) Jung, J. W.; Park, J.-S.; Han, I. K.; Lee, Y.; Park, C.; Kwon, W.; Park, M. Flexible and Highly Efficient Perovskite Solar Cells with a Large Active Area Incorporating Cobalt-Doped Poly(3-hexylthiophene) for Enhanced Open-Circuit Voltage. *J. Mater. Chem. A* **2017**, *5*, 12158−12167.
(54) Huang, D.; Goh, T.; Kong, J.; Zheng, Y.; Zhao, S.; Xu, Z.; Taylor, A. D. Perovskite Solar Cells with a DMSO-Treated PEDOT:PSS Hole Transport Layer Exhibit Higher Photovoltaic Performance and Enhanced Durability. *Nanoscale* **2017**, *9*, 4236−4243.
(55) Sun, Q.; Fassl, P.; Becker-Koch, D.; Bausch, A.; Rivkin, B.; Bai, S.; Hopkinson, P. E.; Snaith, H. J.; Vaynzof, Y. Role of Microstructure in Oxygen Induced Photodegradation of Methylammonium Lead Triiodide Perovskite Films. *Adv. Energy Mater.* **2017**, *7* (20), 1700977.

DOI: 10.1021/acsaem.7b00176
ACS Appl. Energy Mater. 2018, 1, 676−683

(56) Jeon, N. J.; Noh, J. H.; Yang, W. S.; Kim, Y. C.; Ryu, S.; Seo, J.; Seok, S. I. Compositional Engineering of Perovskite Materials for High-Performance Solar Cells. *Nature* **2015**, *517*, 476−480.
(57) Ye, S.; Sun, W.; Li, Y.; Yan, W.; Peng, H.; Bian, Z.; Liu, Z.; Huang, C. CuSCN-Based Inverted Planar Perovskite Solar Cell with an Average PCE of 15.6%. *Nano Lett.* **2015**, *15*, 3723−3728.
(58) Chen, W.; Wu, Y.; Yue, Y.; Liu, J.; Zhang, W.; Yang, X.; Chen, H.; Bi, E.; Ashraful, I.; Grätzel, M.; Han, L. Efficient and Stable Large-Area Perovskite Solar Cells with Inorganic Charge Extraction Layers. *Science* **2015**, *350*, 944−948.
(59) Liu, T.; Chen, K.; Hu, Q.; Zhu, R.; Gong, Q. Inverted Perovskite Solar Cells: Progresses and Perspectives. *Adv. Energy Mater.* **2016**, *6*, 1600457.
(60) Kazim, S.; Ramos, F. J.; Gao, P.; Nazeeruddin, M. K.; Gratzel, M.; Ahmad, S. A Dopant Free Linear Acene Derivative as a Hole Transport Material for Perovskite Pigmented Solar Cells. *Energy Environ. Sci.* **2015**, *8*, 1816−1823.
(61) Qin, P.; Paek, S.; Dar, M. I.; Pellet, N.; Ko, J.; Grätzel, M.; Nazeeruddin, M. K. Perovskite Solar Cells with 12.8% Efficiency by Using Conjugated Quinolizino Acridine Based Hole Transporting Material. *J. Am. Chem. Soc.* **2014**, *136*, 8516−8519.
(62) Qin, P.; Kast, H.; Nazeeruddin, M. K.; Zakeeruddin, S. M.; Mishra, A.; Bauerle, P.; Gratzel, M. Low Band Gap S,N-Heteroacene-Based Oligothiophenes as Hole-Transporting and Light Absorbing Materials for Efficient Perovskite-Based Solar Cells. *Energy Environ. Sci.* **2014**, *7*, 2981−2985.
(63) Zhu, Z.; Xu, J.-Q.; Chueh, C.-C.; Liu, H.; Li, Z. a.; Li, X.; Chen, H.; Jen, A. K. Y. A Low-Temperature, Solution-Processable Organic Electron-Transporting Layer Based on Planar Coronene for High-performance Conventional Perovskite Solar Cells. *Adv. Mater.* **2016**, *28*, 10786−10793.
(64) Zhao, D.; Zhu, Z.; Kuo, M.-Y.; Chueh, C.-C.; Jen, A. K. Y. Hexaazatrinaphthylene Derivatives: Efficient Electron-Transporting Materials with Tunable Energy Levels for Inverted Perovskite Solar Cells. *Angew. Chem., Int. Ed.* **2016**, *55*, 8999−9003.
(65) Gu, P.-Y.; Wang, N.; Wang, C.; Zhou, Y.; Long, G.; Tian, M.; Chen, W.; Sun, X. W.; Kanatzidis, M. G.; Zhang, Q. Pushing Up the Efficiency of Planar Perovskite Solar Cells to 18.2% with Organic Small Molecules as the Electron Transport Layer. *J. Mater. Chem. A* **2017**, *5*, 7339−7344.
(66) Sun, C.; Wu, Z.; Yip, H.-L.; Zhang, H.; Jiang, X.-F.; Xue, Q.; Hu, Z.; Hu, Z.; Shen, Y.; Wang, M.; Huang, F.; Cao, Y. Amino-Functionalized Conjugated Polymer as an Efficient Electron Transport Layer for High-Performance Planar-Heterojunction Perovskite Solar Cells. *Adv. Energy Mater.* **2016**, *6*, 1501534.
(67) Kato, Y.; Ono, L. K.; Lee, M. V.; Wang, S.; Raga, S. R.; Qi, Y. Silver Iodide Formation in Methyl Ammonium Lead Iodide Perovskite Solar Cells with Silver Top Electrodes. *Adv. Mater. Interfaces* **2015**, *2*, 1500195.
(68) Ginting, R. T.; Jeon, M.-K.; Lee, K.-J.; Jin, W.-Y.; Kim, T.-W.; Kang, J.-W. Degradation Mechanism of Planar-Perovskite Solar Cells: Correlating Evolution of Iodine Distribution and Photocurrent Hysteresis. *J. Mater. Chem. A* **2017**, *5*, 4527−4534.
(69) Bi, E.; Chen, H.; Xie, F.; Wu, Y.; Chen, W.; Su, Y.; Islam, A.; Grätzel, M.; Yang, X.; Han, L. Diffusion Engineering of Ions and Charge Carriers for Stable Efficient Perovskite Solar Cells. *Nat. Commun.* **2017**, *8*, 15330.
(70) Brinkmann, K. O.; Zhao, J.; Pourdavoud, N.; Becker, T.; Hu, T.; Olthof, S.; Meerholz, K.; Hoffmann, L.; Gahlmann, T.; Heiderhoff, R.; Oszajca, M. F.; Luechinger, N. A.; Rogalla, D.; Chen, Y.; Cheng, B.; Riedl, T. Suppressed Decomposition of Organometal Halide Perovskites by Impermeable Electron-Extraction Layers in Inverted Solar Cells. *Nat. Commun.* **2017**, *8*, 13938.

DOI: 10.1021/acsaem.7b00176
ACS Appl. Energy Mater. 2018, 1, 676−683